Magnetic Resonance Imaging, Vol. 1, pp. 197–203, 1982
Printed in the USA.

0730–725X/82 $3.00+.00

● *Research Article*

A FLOW VELOCITY ZEUGMATOGRAPHIC INTERLACE FOR NMR IMAGING IN HUMANS

PAUL R. MORAN, PH.D.

Department of Radiology, Bowman Gray School of Medicine, Winston-Salem, North Carolina 27103, USA, and Department of Physics, Radiology and Medical Physics, University of Wisconsin, Clinical Science Center E3/366, Madison, Wisconsin 53706, USA

We describe a flow sensitizing zeugmatographic phase-modulation interlace for NMR-imaging which is exactly analogous to Lauterbur's spatial-location-sensitizing magnetic field gradients. The method may be implemented by minor modification of any NMR-imaging scanner without interfering with its conventional operation, and enables up to 6-D imaging of the joint (spatial-flow) density of spins $\Delta(\vec{r},\vec{v})$. In a special simplification, specific-flow-density, $\langle v(\vec{r})\rangle$, and flow-current–specific-flow-density, $\rho_0(\vec{r})\langle\vec{v}\rangle$, derive directly from "real" and "imaginary" parts of the image reconstruction.

Keywords: **Medical imaging, Nuclear resonance, NMR imaging, Flow, Flow velocity, Phase-modulation-coding, Field-gradient-modulation, Exchange-flow, Flux-rate-flow.**

NMR-IMAGING: INTRODUCTION AND REVIEW

An earlier paper detailed[5] a general theoretical description of the principles underlying and unifying NMR imaging. We review the basics here by way of introduction. The nuclear species of interest is pulse excited by an rf source at frequency ω_{rf}. This generates a distribution of transverse precessing magnetization, $M_\perp(\vec{r})$, in the subject who is placed in a strong static homogeneous magnetic field. A tuned receiver coil senses the emf from the precessing $M_\perp(\vec{r})$; two-phase sensitive demodulators convert the resulting signal rf into free-induction-decay signals, $S_1(t)$ and $S_2(t)$. These FID signals are, respectively, phase-referenced to "cosine" phase of ω_{rf} (to reflect even-parity components of the subject distribution) and to the "sine" phase (to reflect odd-parity components). $S_1(t)$ and $S_2(t)$ may be combined for ease of expression into a complex signal description, $S(t) = S_1(t) + iS_2(t)$. Then $S(t)$ may be written as the spectral transform

$$S(t) = K \int M_\perp(\omega)\, e^{i\omega t}\, d\omega, \tag{1}$$

where

$$\omega = \omega_{LARMOR} - \omega_{rf}, \tag{2}$$

and K is a constant electronic conversion factor. Lauterbur[7] noted that Eq. 1 is of identical form to the spatial Fourier transform for spin-density, $\rho(\vec{r})$,

$$\tilde{\rho}(\vec{q}) = \int \rho(\vec{r})\, e^{-2\pi i\vec{q}\cdot\vec{r}}\, d\vec{r}. \tag{3}$$

If one imposes a field-gradient "link," so that the Larmor frequency is spatially modulated by

$$\omega_{LARMOR} = 2\pi\gamma[H_0 + \vec{G}\cdot\vec{r}], \tag{4}$$

and tunes ω_{rf} to the mean Larmor frequency, $\omega_{rf} = \gamma H_0$, then Eq. 2 gives

$$\omega = [\gamma H_0 - \omega_{rf}]2\pi + 2\pi\gamma\vec{G}\cdot\vec{r} = 2\pi\gamma\vec{G}\cdot\vec{r}. \tag{5}$$

Thus, Eq. 1 converts to

$$S(t) = \int M_\perp(\vec{r})\, e^{2\pi i\gamma G\cdot rt}\, d\vec{r}, \tag{6}$$

and the variable substitution

$$\vec{q} = -\gamma\vec{G}\cdot\vec{r}, \tag{7}$$

RECEIVED 2/11/83; ACCEPTED 3/4/83.
Address correspondence to Paul R. Moran, Department of Radiology, Bowman Gray School of Medicine, Winston-Salem, NC 27103.

together with the notation convention

$$\tilde{S}(\vec{q}) \equiv S[t = (\vec{q}/\gamma\vec{G})], \tag{8}$$

allows Eq. 6 to be reexpressed as

$$\tilde{S}(\vec{q}) = K\int M_{\perp}(\vec{r})\, e^{-2\pi i\vec{q}\cdot\vec{r}}\, d\vec{r}. \tag{9}$$

Observing that Eq. 9 expresses an experimentally observable FID signal precisely in the same form as the expression for the spatial density-of-spins transform of Eq. 3, Lauterbur demonstrated a particularly powerful and general method of NMR-imaging by reconstruction from the transform signal $\tilde{S}(\vec{q})$. He called this mode of NMR-imaging "zeugmotography," from the Greek stem meaning "link" or "yoke," to reflect the link of magnetic field gradient joining spatial-distributions with temporal-signal evolution, according to Eqs. 4–7 above.

In current practice, many variations of Lauterbur's original discovery are practiced; they employ modifications of rf pulsing for spin–echo data FID, temporal modulation of $\vec{G}$ to derive data-collection strategies in Cartesian[6] rather than spherical/polar coordinates, and so on. Yet the basic principle remains unchanged. Of course, when the data chain giving $\tilde{S}(\vec{q})$ is acquired, sampled, digitized, and stored for later numerical reconstruction, the data experience apodization by various intrinsic effects and by algorithmically imposed bandpass shaping functions. The image, $\mathcal{I}(\vec{r})$, reconstructed from Eq. 9, by numerical discrete Fourier inversion in a variety of geometries, is given by

$$\mathcal{I}(\vec{r}) = \int \tilde{H}(\vec{q})\tilde{S}(\vec{q})\, e^{2\pi i\vec{q}\cdot\vec{r}}\, d\vec{q}, \tag{10}$$

where $\tilde{H}(\vec{q})$ is the apodizing function appropriate to the system.

Again comparing Eqs. 3 and 9, we observe that the precessing magnetization distribution, $M_{\perp}(\vec{r})$, is directly proportional to spin-density, $\rho(\vec{r})$, but modulated by relaxation rate factors (T_1 and T_2 relaxation phenomena) and by details of the rf pulse sequence. We noted previously[11,12] that all such modulation terms, including coil-geometry sensitivity factors, could be gathered into a single definition of "effective" spin-density, ρ_{eff}, so that

$$\tilde{S}(\vec{q}) = K\int \rho_{\text{eff}}(\vec{r})\, e^{-2\pi i\vec{q}\cdot\vec{r}}\, d\vec{r}, \tag{11}$$

and Eq. 10 becomes

$$\mathcal{I}(\vec{r}) = K\int \tilde{H}(\vec{q})\tilde{\rho}_{\text{eff}}(\vec{q})\, e^{2\pi i\vec{q}\cdot\vec{r}}\, d\vec{q}. \tag{12}$$

Whence $\mathcal{I}(\vec{r})$ is a blurred-image representation of the effective spin-density distribution,

$$\begin{aligned}\mathcal{I}(\vec{r}) &= \int \text{psf}(\vec{r}')\rho_{\text{eff}}(\vec{r} - \vec{r}')\, d\vec{r}' \\ &\equiv \text{psf} \otimes \rho_{\text{eff}}(\vec{r}),\end{aligned} \tag{13}$$

where

$$\text{psf}(\vec{r}) = H(\vec{r}) = \int \tilde{H}(\vec{q})\, e^{2\pi i\vec{q}\cdot\vec{r}}\, d\vec{q}. \tag{14}$$

Consequently, the general method of NMR-imaging is that a series of data collection cycles occur. In each data cycle, a particular gradient sequence causes a particular line of $\tilde{S}(\vec{q})$ to evolve tracing out a line-sampling in $\vec{q}$-space. From cycle to cycle, $\vec{G}$ varies to modify the $\vec{q}$-line acquired, until a sufficiently dense sampling[5] of $\tilde{S}(\vec{q})$ is obtained. Then $\mathcal{I}(\vec{r})$ is reconstructed by numerically calculating the Fourier inversion result given by Eq. 12 on some specified pixel-mesh chosen for a discrete set of $\vec{r}$ positions. While the specifics of the numerical programs may differ in detail, depending upon the particular data-collection strategies used, all have the same unifying and common principles. All submodes use a field-gradient encoding of frequency to spatial distribution according to Eqs. 4–9 for the FID data and then a Fourier inversion according to Eqs. 10–12 for image reconstruction. In this sense, only the very early "sensitive-point" types of NMR-imaging (which are point-by-point methods, and which are inefficient in data collection rates, and which suffer enormous signal-to-noise disadvantages) differ in any significant way from the zeugmatography mode originally proposed by Lauterbur.

Anticipating subsequent discussion, we here make two additional observations. First, the data apodizing function, $\tilde{H}(\vec{q})$, may simply be absorbed, along with the electronic conversion factor, K, into a definition of the NMR-image spin-density, $\rho_0(\vec{r})$,

$$\begin{aligned}\tilde{\rho}_0(\vec{q}) &\equiv K\tilde{H}(\vec{q})\, \tilde{\rho}_{\text{eff}}(\vec{q}) \\ &\equiv \tilde{H}(\vec{q})\, \tilde{S}(\vec{q}),\end{aligned} \tag{15}$$

so that the Fourier inversion expression of Eq. 12 gives

$$\mathcal{I}(\vec{r}) = \int\tilde{\rho}_0(\vec{q})\, e^{2\pi i\vec{q}\cdot\vec{r}}\, d\vec{q} = \rho_0(\vec{r}). \tag{16}$$

Second, in general, $\mathcal{I}(\vec{r})$ as given by Eq. 16, comprises two parts:

$$\mathcal{I}(\vec{r}) = I(\vec{r}) + iJ(\vec{r}), \tag{17}$$

and, in the specific cases described above, the real physical nature of $\rho_{\text{eff}}(\vec{r})$ guarantees the Hermetian property, $\tilde{S}(-\vec{q}) = \tilde{S}^*(\vec{q})$. Consequently, if there are no phase-errors influencing $\tilde{H}(\vec{q})$, the "imaginary" part of Eq. 16 (in Eq. 17) returns a null value,

$$J(\vec{r}) = 0 \text{ everywhere.} \tag{18}$$

MEDICAL APPLICATIONS

The physics governing NMR phenomena and the macroscopic biophysics inherent in subjects of medical interest impose constraints on detected signal levels. NMR-imaging has extremely low signal-to-noise ratios in the image in relation to analogous X-ray modalities, e.g., X-ray CT-scan images, when one compares intrinsic SNR for equal resolving powers and equal scanning times. For example, an X-ray CT-scan of a patient's head may be ordered to study the morphology of the ventricles filled with cerebrospinal fluid against a background of normal brain tissue. A 2 mm tomographic slice thickness, having planar image resolving-power exceeding 5 line-pairs per centimeter, and with quantum statistics limited noise precision in the image of a few tenths of one percent of the normal density of water, commonly results from a 4–5 sec CT scan. The exposure-area-product at the patient's skin, under these conditions, need not exceed a rather modest $2\text{–}4 \times 10^{-3}$ R-m^2, less than about one week's normal exposure to natural background radiation.

To attain comparable NMR images, one would require at least several tens of minutes of scanning time. At these scan times, the NMR-image would probably be limited in quality, in medical practice, by patient motion artifacts and blurring. The severe limitations of NMR-imaging with respect to X-ray modalities, when one is concerned purely with morphological images and anatomic detail, were first pointed out explicitly to us by Lauterbur.[8] He emphasized, however, that the truly unique aspect of NMR scans in medical application was *not* in display of simple morphology, but rather resided in NMR's potential for imaging physiological and functional information, and credited Damadian's work[2] as one example. Damadian had demonstrated that neoplasms might show T_1 and/or T_2 relaxation behaviors significantly different from normal tissues of the same type, and that such information from an in vivo study was probably not otherwise obtainable.

Unfortunately, in applications to medical imaging, these hopeful potentials of NMR have largely remained unrealized. This doubtlessly is a major contributing reason why X-ray CT and NMR-imaging, analagous modalities of similar complexity both initiated in the early 1970's, subsequently demonstrated such a great disparity in their rates of development for clinical application in human medical studies.

For example, the flow of fluids in a human subject is a most important phenomena, and its measure and imaging would provide diagnostic medicine with invaluable information for functional assessment and physiological status. Work on NMR blood "flowmeters" began in the mid-1950's[13] and attempts to extend and improve flow related measurements in NMR-imaging modes have been pursued by various groups.[1,3,4,13,15] These methods have been based upon relatively subtle time-of-flight NMR signal perturbations which may somewhat influence the reconstructed image. These flow-related image phenomena appear to be caused by T_1-saturation effects in slice-oriented imaging strategies or due to some apodizing effects generated by flowing spins in the presence of the imaging-gradient-fields, $\vec{G}$, discussed in the previous section. Although research into their utilization continues, these NMR-imaging flow effects have not so far appeared to be sufficiently reliable or interpretable to provide solid demand for clinical applications.

The following section describes a novel "velocity-zeugmatographic" method which enables direct and quantitative NMR imaging of true flow. In this case, the link is a special NMR phase-modulation sequence; it interlaces with the "spatial-zeumatographic" imaging-gradient sequence. It specifically sensitizes to flow velocity of excited magnetization in a manner precisely analagous to Lauterbur's field-gradient sensitization to spatial location; but it also is physically "orthogonal" to the imaging-gradients and thus completely independent of them.

VELOCITY ZEUGMATOGRAPHY

Describing flow

We generalize the spin-density function to a distribution in six dimensions, three spatial variables and three velocity variables. We call this density $\Delta(\vec{r}, \vec{v})$; as before, we absorb T_1 and T_2 modulations and image-blurring in our definition of $\Delta_0(\vec{r}, \vec{v})$,

$$\Delta_0(\vec{r},\vec{v}) = \text{effective blurred number of spins per unit spatial volume and per unit velocity volume, at location } \vec{r} \text{ and with velocity } \vec{v}. \tag{19}$$

The spatial density, $\rho_0(\vec{r})$, is given by

$$\rho_0(\vec{r}) = \int \Delta_0(\vec{r}, \vec{v})\, \mathrm{d}\vec{v}, \tag{20}$$

while the corresponding spatially "averaged" velocity

distribution, $D_0(\vec{v})$, is

$$D_0(\vec{v}) = \int \Delta_0(\vec{r}, \vec{v})\, d\vec{r}. \quad (21)$$

Just as we earlier denoted a spatial wave vector by $\vec{q}$ and considered the transform pair $\rho_0(\vec{r})$ and $\tilde{\rho}_0(\vec{q})$, we can specify a "velocity wave vector" by $\vec{f}$ and consider the transform pair, $D_0(\vec{v})$ and $\hat{D}_0(\vec{f})$. We use the "tilde" notation for the spatial transform and the "caret" notation for velocity transform. We also can describe the joint density and its transform by

$$\hat{\tilde{\Delta}}_0(\vec{q}, \vec{f}) = \int\int \Delta_0(\vec{r}, \vec{v})\, e^{-2\pi i[\vec{q}\cdot\vec{r}+\vec{f}\cdot\vec{v}]}\, d\vec{r}\, d\vec{v}, \quad (22)$$

and

$$\Delta_0(\vec{r}, \vec{v}) = \int\int \hat{\tilde{\Delta}}_0(\vec{q} \cdot \vec{f})\, e^{2\pi i[\vec{q}\cdot\vec{r}+\vec{f}\cdot\vec{v}]}\, d\vec{q}\, d\vec{f}. \quad (23)$$

Lauterbur's NMR spatial zeugmatographic principle employed a spatial imaging gradient, $\vec{G}$, to modulate the FID signals so that

$$\phi(\vec{r}) \equiv -2\pi\vec{q} \cdot \vec{r} = 2\pi\gamma\vec{G} \cdot \vec{r}t. \quad (24)$$

For flow sensitized NMR imaging we require an analogous principle to generate a velocity phase modulation, $\theta(\vec{v}) = 2\pi\vec{f} \cdot \vec{v}$, which explicitly is independent of spatial location. Consider the NMR phase modulation integral,[10] arising from a temporally modulated flow-sensitizing field gradient, $\vec{F}(t)$,

$$\theta(\vec{v}) = \int_0^\infty 2\pi\gamma\vec{F}(t') \cdot [\vec{r} + \vec{v}t']\, dt', \quad (25)$$

where $\vec{F}(t)$ must be selected so that θ does not depend upon $\vec{r}$. It is clear that any modulation such that

$$\int \vec{F}(t')\, dt' = 0, \quad (26)$$

accomplishes the removal of dependence upon $\vec{r}$. The flow zeumatography modulation which is apparent as also giving the greatest $\vec{v}$ dependence is*

$$\vec{F}(t) = \begin{cases} \vec{F}; t_0 - \tau \le t < t_0 \\ -\vec{F}; t_0 \le t \le t_0 + \tau. \end{cases} \quad (27)$$

In this case, Eq. 25 gives

$$\theta(\vec{v}) = 2\pi\gamma\tau^2\vec{F} \cdot \vec{v} \equiv -2\pi\vec{f} \cdot \vec{v} \quad (28)$$

in complete complementarity to Lauterbur's relation in Eq. 24. Figure 1 schematically shows one example of a single cycle of NMR data collection where $\vec{F}(t)$ interlaces the imaging-gradient sequence.

That NMR imaging of true flow is ordinarily unattainable because only turbulence or diffusive motion generates loss of phase coherence recently was noted by Grant and Back.[3] In the velocity-zeugmatography concept described above, however, we make explicit use of this fact to generate a flow specific phase modulation. If we then create a series of imaging cycles so that

$$\vec{F} = nF_0\hat{x} + mF_0\hat{y} + lF_0\hat{z}, \quad (29)$$

where $(n, m, l) = 0, \pm1, \pm2, \pm3 \ldots$, and accumulate data, then we can implement a "6-D" discrete Fourier inversion and reconstruct $\Delta_0(\vec{r}, \vec{v})$,

$$\Delta_0(\vec{r}, \vec{v}) = K\int\int \tilde{H}_s(\vec{q})\hat{H}_v(\vec{f})\tilde{S}(\vec{q}, \vec{f})\, e^{2\pi i(\vec{q}\cdot\vec{r}+\vec{f}\cdot\vec{v})} d\vec{q}\, d\vec{f}$$

$$= \int\int \hat{\tilde{\Delta}}_0(\vec{q}, \vec{f})\, e^{2\pi i(\vec{q}\cdot\vec{r}+\vec{f}\cdot\vec{v})}\, d\vec{q}\, d\vec{f}. \quad (30)$$

This 6-D image has its resolution of the flow-spectroscopy of $\vec{v}$ determined by $\hat{H}_v(\vec{f})$ in Eq. 30, which essentially is limited by the maximum values of the magnitude of $\vec{f}$ in Eq. 28 as governed by the range (n, m, l) (in Eq. 29) used in the series of $\vec{F}$ cycles. Reciprocally, one can encompass a range of velocities, $|\vec{v}| < v$:max, by choosing

$$\gamma F_0\tau^2 \lesssim [v\text{:max}]^{-1}. \quad (31)$$

Simplifications

Of course, the full 6-D image considered above represents the most general and ambitious form of direct imaging of true flow velocities, although it is fairly obvious how other variables, such as chemical shift distributions or T_1 and T_2 spectroscopy might be added and similarly interlaced in the data-collection cycle as well. Restricting, however, current consideration to spin–flow, there are many potentially useful drastic simplifications of the technique. For example, only a single $\vec{F}$-gradient direction need be used (e.g., $n = m = 0$ always, in Eq. 29) and one would then reconstruct directly

$$\Delta_0(\vec{r}; v_z) = \int \Delta_0(\vec{r}; v_x, v_y, v_z)\, dv_x\, dv_y. \quad (32)$$

*It also is apparent[10] that, even for scanners which have no current field-gradient reversal capability and must rely upon 180°-pulse spin–echos for $\tilde{S}(\vec{q})$ and $\tilde{S}(-\vec{q})$ data, an equivalent bipolar-phase-modulation occurs when one applies two equivalent $\vec{F}$ unipolar pulses with an intervening 180°-rf-pulse to accomplish the phase reversal needed.

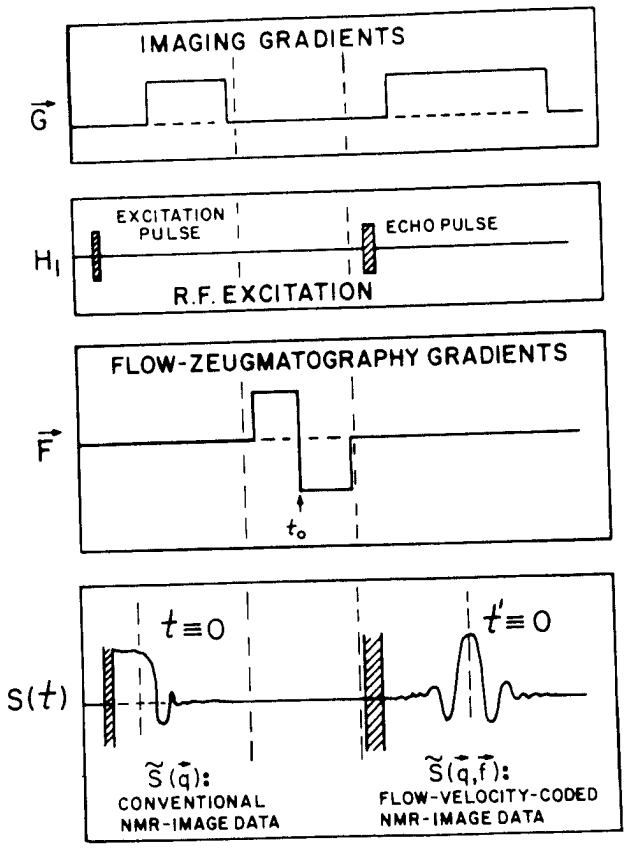

Fig. 1. An example of one possibility for the flow-zeugmatography phase-modulation interlace into a conventional imaging-gradient cycle.

Further, since the $\vec{F}(t)$ modulation gives velocity specific phase shifts orthogonal in representation to the spatial-to-frequency encoding function of the conventional imaging-gradients, $\vec{G}$, this mode of flow-imaging can join, in any of its forms, with any conventional submode of NMR imaging. The only essential is that some bipolar $\vec{F}(t)$ phase-modulation be applied subsequent to rf excitation, but prior to acquisition of FID-image data which it is to sensitize. Thus, it may be applied in various ways not only to "conventional" 2-D and 3-D zuegmatographic modes (whatever their data-collection strategies, including multiecho techniques such as Mansfield's[9] planar–echo), but also to various "sensitive-point" imaging modes. One also can imagine hybrid flow imaging; for example, a broad-slice-selection rf sequence could be followed by flow-sensitizing modulation and then data collected in "broad-sensitive-line" a.c. field-gradients to isolate a single organ spatial region-of-interest. One could then display a "velocity-image" (in distinction to an image of velocity), where the display coordinates represent $\vec{v}$ (not $\vec{r}$) and the display brightness represents the number of spins having that value of $\vec{v}$, all for that particularly selected sensitive-volume.

It would appear that there is an endless variety of modifications and simplifications by which the flow-zuegmatographic phase-modulation principle can be applied to studies of practical importance. In medical imaging, it would seem limited only by successful identification of the flow quantity of clinical interest, and by the ingenuity, imagination and perhaps, the patience of the NMR-scanner's operator. In the final section we consider a special case of flow-imaging which is very useful when one desires only to measure the specific-flow-density, $\langle \vec{v}(r) \rangle$ and/or the flow-current-density $\rho_0(\vec{r})\langle \vec{v} \rangle$.

SIMPLIFICATION TO SPECIFIC FLOW

Flow quantities

In medical assessment, we may consider two gross flow quantities of interest. The first we define as exchange-flow, W_f, and it is the inverse of the exchange time of molecules out of (or into) some specified volume, V. Let this volume be defined by its closed surface, $A(\vec{r})$; and let a differential increment of that surface area be represented by $\mathrm{d}\vec{A}$,

$$\mathrm{d}\vec{A} = \mathrm{d}A\hat{n}. \tag{33}$$

In Eq. 33, $\mathrm{d}\vec{A}$ is the differential area vector and $\hat{n}$ is the outwardly directly unit-vector normal to the surface at that point. The average outflow current, $\rho_0\langle v_n \rangle$, at $\mathrm{d}\vec{A}$ is

$$\rho_0(\vec{r})\langle v_n \rangle = \int_0^\infty \Delta_0(\vec{r}, \vec{v})[\vec{v} \cdot \hat{n}]\, \mathrm{d}\vec{v}, \tag{34}$$

whence we determine the exchange-flow for volume, V, bounded by A according to

$$W_f = \oint_{\mathrm{SURF}} \left\{ \int_0^\infty \Delta_0(\vec{r}, \vec{v})[\vec{v} \cdot \mathrm{d}\vec{A}]\, \mathrm{d}\vec{v} \right\}. \tag{35}$$

The previous section shows how to measure $\Delta_0(\vec{r}, \vec{v})$ everywhere in principle, so programs implemented in the system's software can enable calculation of W_f for any arbitrary volume. There also are technique simplifications, beyond the scope of this paper, which can give appropriate estimates of W_f without the need to fully acquire $\Delta_0(\vec{r}, \vec{v})$.

A second flow quantity is what we may call the flux-rate-flow, F. Consider some arbitrary (unclosed) surface, Ω, and a directed differential element of it, $\mathrm{d}\vec{\Omega}$. If we calculate the flow-current-density, $\rho_0\langle \vec{v} \rangle$,

$$\rho_0(\vec{r})\langle \vec{v} \rangle \equiv \int_\infty^\infty \vec{v}\Delta_0(\vec{r}, \vec{v})\, \mathrm{d}\vec{v}, \tag{36}$$

then the flux–flow through Ω is given by

$$F(\Omega) = \int_{\Omega} \rho_0(\vec{r})\langle\vec{v}\rangle \cdot d\vec{\Omega}. \tag{37}$$

We also may speak of the normalized flow-quantities corresponding to $W_f(V)$ and $F(\Omega)$. Whereas W_f and F give the number of molecules per second, and reference the density $\rho_0(\vec{r})$ at their respective surfaces, both may be normalized to the volume flow quantities w_f and f by

$$w_f(V) \equiv W_f(V)\rho_0^{-1}, \tag{38}$$

and

$$f(\Omega) \equiv F(\Omega)\rho_0^{-1}. \tag{39}$$

In Eqs. 38 and 39, ρ_0 is the average number density of the entities of interest determined at the particular surface (or within the particular volume) of interest. It is clear that a complete determination of $\Delta_0(\vec{r},\vec{v})$ allows calculation of $W_f(V)$ and $F(\Omega)$ and $w(v)$ and $f(\Omega)$ everywhere. If, however, we could measure the specific-flow-density, $\langle\vec{v}(\vec{r})\rangle$, directly then calculation of $f(\Omega)$ would greatly be simplified,

$$f(\Omega) = \int_{\Omega} \langle\vec{v}(\vec{r})\rangle \cdot d\vec{\Omega}, \tag{40}$$

and if we could measure $\rho_0(\vec{r})\langle\vec{v}\rangle$ (the flow-current-density) directly, then determination of $F(\Omega)$ is simply made directly from the definition in Eq. 37.

A special case

We can evaluate the flow-current-density of Eq. 36 from the reconstruction expression of Eq. 30 and express it in the form

$$\begin{aligned}\rho_0(\vec{r})\langle\vec{v}\rangle &= \int \left[\int \vec{v}\hat{\Delta}_0(\vec{r},\vec{f})\, e^{2\pi i\vec{f}\cdot\vec{v}}\, d\vec{f}\right] d\vec{v} \\ &= [2\pi i]^{-1}\,[\vec{\nabla}_f \hat{\Delta}_0(\vec{r},\vec{f}\,]\vec{f}\rightarrow 0.\end{aligned} \tag{41}$$

We obtain a good approximation for Eq. 41 by employing a single-flow-sensitizing modulation within a complete series of $\vec{G}$ cycles to acquire data for

$$\begin{aligned}\hat{\Delta}_0(\vec{r},\vec{f}_1) &= \int \Delta_0(\vec{r},\vec{v})\, e^{-2\pi i\vec{f}_1\cdot\vec{v}}\, d\vec{v} \\ &\equiv \int \Delta_0(\vec{r},\vec{v})\, e^{i\theta_1(\vec{v})}\, d\vec{v},\end{aligned} \tag{42}$$

where $\theta_1(\vec{v})$ is given by Eq. 28

$$\theta_1(\vec{v}) = 2\pi\gamma\tau^2\vec{F}_0 \cdot \vec{v}. \tag{43}$$

if we maintain $F_0\tau^2$ small, so that

$$e^{i\theta_1(\vec{v})} \approx (1 + 2\pi i\gamma\tau^2\vec{F}_0 \cdot \vec{v}), \tag{44}$$

then Eq. 42 gives

$$\begin{aligned}\hat{\Delta}_0(\vec{r},\vec{f}_1) &= \int \Delta_0(\vec{r},\vec{v})\, d\vec{v} + i2\pi\gamma\tau^2\vec{F}_0\int \vec{v}\Delta_0(\vec{r},\vec{v})\, d\vec{v} \\ &= \rho_0(\vec{r}) + i2\pi\gamma\tau^2\vec{F}_0[\rho_0(\vec{r})\langle\vec{v}\rangle],\end{aligned} \tag{45}$$

and this has a direct interpretation as the image reconstruction of $\mathcal{J}(\vec{r})$ according to Eq. 17. That is, by applying the bipolar flow phase-modulation interlace in Fig. 1, with small $2\pi\gamma\tau^2F_0$, for a single $\vec{F}_0$ and a conventional series of $\vec{G}$ cycles, we can immediately reconstruct an image $\mathcal{J}_F(\vec{r})$ having

$$\mathcal{J}_F(\vec{r}) = I(\vec{r}) + iJ_F(\vec{r}). \tag{46}$$

In Eq. 46 we have, according to Eq. 45,

$$I(\vec{r}) = \rho_0(\vec{r}), \tag{47}$$

which is the conventional* image, and by continuing the reconstruction to produce the imaginary-part as well, we find

$$J_F(\vec{r}) = (2\pi\gamma\tau^2\vec{F}_0)[\rho_0(\vec{r})\langle\vec{v}\rangle]. \tag{48}$$

Since all quantities in the parentheses of Eq. 48 are experimentally known, $\text{im:}\mathcal{J}_F(\vec{r}) = J(\vec{r})$ returns any component of flow current density

$$[J(\vec{r})/2\pi\gamma\tau^2F_0] = \rho_0(\vec{r})\langle v_0\rangle, \tag{49}$$

while $\text{re:}\mathcal{J}_F(\vec{r}) = I(\vec{r})$ is the conventional image of $\rho_0(\vec{r})$; normalizing the image of Eq. 49 by $I(\vec{r})$ in Eq. 47, we generate the image of specific-flow-density component along $\vec{F}_0$, $\langle v_0\rangle$,

$$[J(\vec{r})/I(\vec{r})2\pi\gamma\tau^2F_0] = \langle v_0(\vec{r})\rangle. \tag{50}$$

Thus, this simple special case may be employed to obtain direct images of $\rho_0(\vec{r})$, $\rho_0(\vec{n})\langle\vec{v}\rangle$, and $\langle\vec{v}\rangle$ via $\text{re:}\mathcal{J}_F(\vec{r})$, $\text{im:}\mathcal{J}_F(\vec{n})$, and their point-by-point ratio.

*Since the bipolar modulation give a specific phase-shift modulation, it is evident that the spatial-image information must have *measured*, not calculated, values for both $+q$ and $-q$, and that the modulus, $[\mathcal{J}_F\mathcal{J}_F^*]^{1/2}$, always returns exactly $[\rho_0^2]^{1/2}$.

Relatively simple "region-of-interest" software routines then could be used to calculate volume-flow, of $f(\Omega)$, (from Eq. 40) and current-flow, $F(\Omega)$, (from Eq. 37) for any arbitrary surface, Ω, indicated by the system operator.

SUMMARY

Local average flow and often, its velocity distribution can be among the most important physiological and functional qualities to determine and display as an image in many crucial areas of medical diagnosis and assessment of function. In this paper, we have shown how to interlace (in addition to and analogous to Lauterbur's spatial zeugomatic field gradients) a flow-zeugmatographic phase modulation field-gradient into a conventional NMR data-collection cycle and, thereby, obtain full quantitative direct images of true flow. In a special case, we discuss a simplification whereby any vector sense of specific-flow-density, $\langle \vec{v}(\vec{r}) \rangle$, and flow-current-density, $\rho_0(\vec{r})\langle \vec{v} \rangle$, can be imaged immediately from the real and imaginary parts of an NMR-image reconstruction. This method can be implemented by obvious minor modifications on any NMR-imaging scanner and does not interfere with its conventional operation. The ordinary NMR-images remain intact, and the additionally resulting flow-zeugmatographic images suffer no constraints beyond the limitations already extant for conventional NMR-imaging. We hope that true flow NMR-imaging will prove to be one of the direct functional imaging modes enabling NMR to realize some of its vast potential in clinical application to human medical study.

REFERENCES

1. Battocletti, J.H.; Halbach, R.E.; Knox, T.A.; Sances, A. A method of flow imaging, Proc. Society of Magnetic Resonance in Medicine, Boston, MA; 1982.
2. Damadian, R. *Science* 171:1151; 1971.
3. Grant, J.P.; Back, C. *Med. Phys.* 9(2):188; 1982.
4. Kaufman, L. Reading the NMR image. *Diagnostic Imaging,* Nov: 28; 1982.
5. King, K.F.; Moran, P.R. A unified description of NMR-imaging, data collection strategies, and reconstruction (submitted to *Med. Phys.*). Available as University of Wisconsin Medical Physics Technical Report (Dept. of Medical Physics, 1530 Med. Sci. Center, Univ. of Wisconsin, Madison, WI 53706) December 1982. Also King, K.F., Ph.D. Thesis, Univ. of Wisconsin, Dept. of Physics (1982), University Microfilms, Ann Arbor, Michigan
6. Kumar, A.; Welti, D.; Ernst, R.R. *J. Magn. Reson.* 18:69; 1975.
7. Lauterbur, P.C. *Nature* 242:190; 1973. See also Lauterbur, P.C. *Pure Appl. Chem.* 40(2); 1975.
8. Lauterbur, P.C. Private Communication, Medical Physics Seminar Series, the University of Wisconsin; 1976.
9. Mansfield, P.; Maudsley, A.A. *J. Phys. C. Solid State Phys.* 9; 1976.
10. Moran, P.R. *J. Chem. Phys. Solids* 30:297; 1968.
11. Moran, P.R. Development of tissue-like materials for NMR phantoms, Proc. First Workshop on NMR Imaging, Houston, Texas; 1981 (available as for Ref. 5).
12. Moran, P.R. Fundamentals and significance of NMR quantities for application in medical imaging, Proc. Second Workshop NMR Imaging, Houston, Texas; 1982 (available as for Ref. 5).
13. Singer, J.R. *Science* 130:1652; 1959.
14. Singer, J.R. NMR flow imaging, Proc. NMR Imaging Int. Symposium, Bowman Gray School of Medicine, Winston-Salem, NC; 1981.
15. Van As, H.; Schaafsma, T.J. Non-invasive blood flow measurements, Proc. Society of Magnetic Resonance in Medicine, Boston, MA; 1982.